International Journal Of Engineering Research And Development
e-ISSN: 2278-067X, p-ISSN: 2278-800X, www.ijerd.com
Volume 13, Issue 9 (September 2017), PP.12-19

CFD Analysis for Thermal Behavior of Turbulent Channel Flow of Different Geometry of Bottom Plate

[*]Rohit Joshi[1], Dr. Satyendra Singh[2]

[1] *PG Scholar, Department of Mechanical Engineering, BTKIT Dwarahat*
[2]*Associate Professor & Head, Department of Mechanical Engineering, BTKIT Dwarahat*
Corresponding Author: [*]Rohit Joshi

ABSTRACT: The present work is carried out to investigate heat transfer and friction factor characteristics of fluid (air) flow through turbulent channel i.e. parallel plate heat exchanger for different geometry and designs parameters, with a bottom plate applied to uniform constant heat flux thermal boundary condition, and upper plate is provided with a insulated condition. The fluid domain is designed using ANSYS Workbench v15 software and simulated using ANSYS Fluent v15 software, which is based on finite element method. Realizable k-ε turbulent model with wall function is applied for solving turbulence in the domain, and second-order upwind scheme was provided for calculation. The SIMPLE algorithm was adopted to handle the pressure-velocity coupling in the calculation. Parameters like Nusselt number, friction factor and heat transfer coefficient have been obtained for the designs and different contours of temperature, turbulent kinetic energy and velocity magnitude are also presented. The geometries used for bottom plate of heat exchanger are trapezoidal grooved, ribbed and rib-grooved plate, and the groove/rib length (B) to channel height (H) ratio are taken as 0.5, 0.75, 1.0, 1.25 and 1.5 for all three geometry and simulation is done for turbulent regime from 6000 to 18000 Reynolds number . The main objective is to find optimum B/H ratio under similar boundary condition. The optimum B/H ratio are found according to thermal analysis of trapezoidal grooved, ribbed and rib-grooved is 1.0, 1.25 and 1.5 respectively at Reynolds number is 6000.

Keyword: Turbulent channel, ANSYS Fluent, 2-D Analysis, Different geometries, Friction Factor

I. INTRODUCTION

The improvement of convective heat transfer in thermal systems is needed in many engineering applications with a view to reducing the size, weight and cost of heat exchangers. Attempts have been made to enhance heat transfer in the heat exchangers by using roughen surfaces or turbulators such as rib, groove and helical rib in disturbing the flow and in providing transverse/longitudinal vortices or three dimensional mixing. Comprehensive reviews on heat transfer enhancement by periodic surfaces mounted obstacles have rarely been found because of the wide variability of geometric parameters A review of measurements of global heat transfer coefficient and pressure drop for various rib configurations was given by Dalle Donne and Meyer [1]. Martin and Bates [2] presented velocity field and the turbulence structure in an asymmetrically ribbed rectangular channel with one rib configuration of square ribs and varying channel height. Hong and Hsieh [3] investigated the influence of rib alignment on forced convection in a channel at different rib alignments, either staggered or in-line, on the internal surfaces of rectangular or square channels. Jaurker et al. [4] reported the heat transfer and friction characteristics of rib–grooved artificial roughness on one broad heated wall of a large aspect ratio duct. Distributions of the heat transfer coefficient and the pressure drop along the wall inside an asymmetrically ribbed channel measured for thermally developing and turbulent flow over periodic grooves were studied by Lorenz et al. [5]. Numerical investigations on turbulent flow friction and heat transfer enhancement in ducts or channels with rib, groove or rib–groove turbulators have been carried out extensively. Chaube et al. [6] investigated the flow and heat transfer characteristics of a two dimensional rib roughened rectangular duct with only one principal heating wall by using the shear stress transport k−ω turbulence model. Saidi and Sunden [7] studied the thermal characteristics in a duct with rib turbulators by using a simple eddy viscosity model and an explicit algebraic stress model and reported that the algebraic stress model has some superiority over the eddy viscosity model for only velocity field structure prediction. Tatsumi et al. [8] investigated numerically the flow around a discrete rib attached obliquely to the flow direction onto the bottom wall of a square duct and found that noticeable heat transfer augmentation was obtained downstream of the rib, produced by a strong secondary flow motion. Yang and Hwang [9] numerically examine the heat transfer enhancement in rectangular ducts with slit and solid ribs.

2. Geometry of the present problem

The geometry is made for analysis are different types of turbulent channel having protruded bottom plate which are made up of aluminum having length 1.88m and hydraulic diameter of 0.08m in which internal fluid flow occurs.

Protrusions made in bottom plate of three different channels are as follows:-

1. Plate with groove having 9 grooves.
2. Plate with groove having 9 grooves.
3. Plate with rib-groove, 4 ribs and 5 grooves.

Turbulent channel consist of three sections:

1. Entry section
2. Test section
3. Exit section

The geometries of ribbed, grooved and rib-grooved channel are shown in fig. 1-3.

Table 1: Geometrical data of the model

Total length (m)	1.88
Entry length (m)	0.8
Test section length(m)	0.68
Exit length (m)	0.4
Distance between two plates H, (m)	0.04
Groove depth T, (m)	0.02
Rib height T, (m)	0.02
Groove length B, (m)	0.02, 0.03, 0.04, 0.05, 0.06
Rib length B, (m)	0.02, 0.03, 0.04, 0.05, 0.06

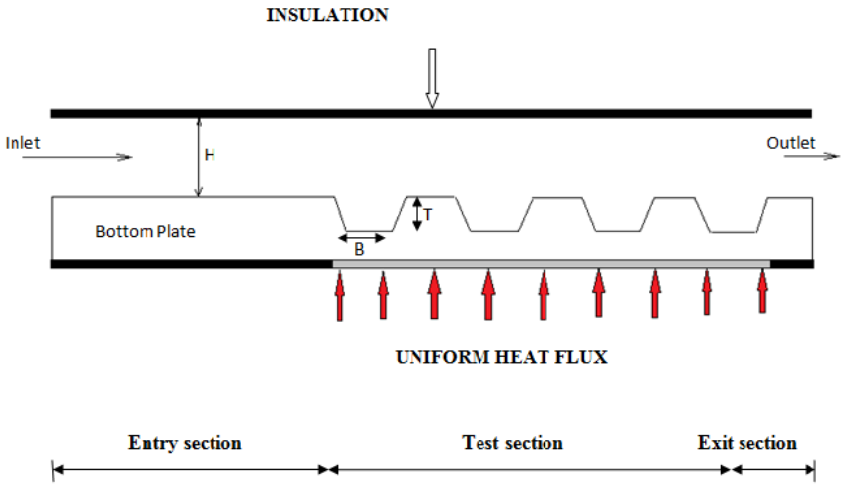

Fig 1 Schematic diagram for grooved channel

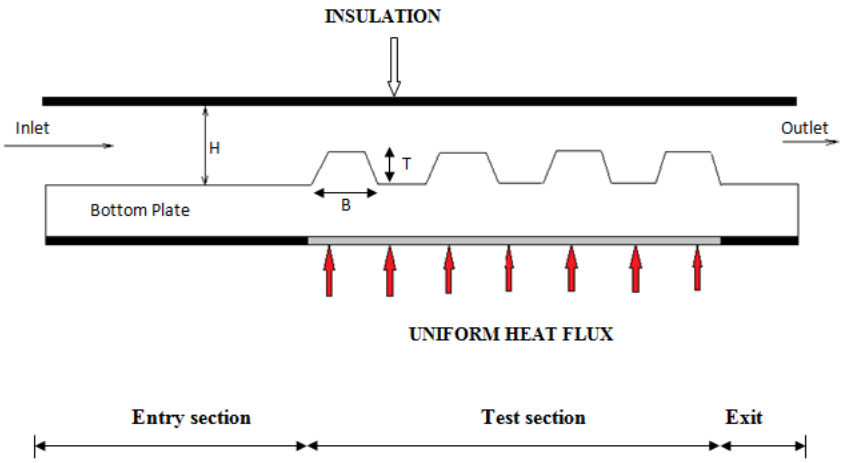

Fig 2 Schematic diagram for ribbed channel

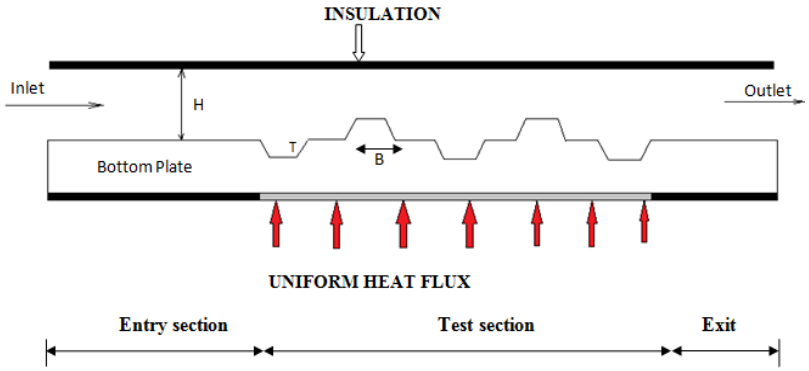

Fig 3 Schematic diagram for rib-grooved channel

II. MATHEMATICAL MODELING

3.1. Flow governing equations

The phenomenon under consideration is governed by the steady 2-D form of the continuity, the time-averaged incompressible

Navier–Stokes equations and the energy equation. In the Cartesian tensor system these equations can be written as:

Continuity equation:

$$\frac{\partial}{\partial x_i}(\rho u_i) = 0 \qquad (1)$$

Momentum equation:

$$\frac{\partial(\rho u_i u_j)}{\partial u_j} = -\frac{\partial p}{\partial x_i} + \frac{\partial}{\partial x_j}\left[\mu\left(\frac{\partial u_i}{\partial x_j} + \frac{\partial u_j}{\partial u_i}\right)\right] + \frac{\partial}{\partial x_j}\left(-\rho u_i u_j\right) \qquad (2)$$

Energy equation:

$$\frac{\partial}{\partial x_i}(\rho u_i T) = \frac{\partial}{\partial x_j}\left((\tau + \tau_t)\frac{\partial T}{\partial x_j}\right) \qquad (3)$$

Where τ and τ_t are molecular thermal diffusivity and turbulent thermal diffusivity, respectively and are given by

$$\tau = \frac{\mu}{Pr}, \text{ and } \tau = \frac{\mu_t}{Pr_t} \qquad (4)$$

The Reynolds-averaged approach to turbulence modeling requires that the Reynolds stresses, $-\rho u_i u_j$ in Eq. (2) needs to be modeled. For closure of the equations, the k−ε turbulence model is chosen. A common method employs the Boussinesq hypothesis to relate the Reynolds stresses to the mean velocity gradients:

$$-\rho u_i' u_j' = \mu\left(\frac{\partial u_i}{\partial u_j} + \frac{\partial u_j}{\partial u_i}\right) \qquad (5)$$

The turbulent viscosity term μ_t is to be computed from an appropriate turbulence model. The expression for the turbulent viscosity is given as

$$\mu_t = \rho C_\mu \frac{K^2}{\varepsilon} \qquad (6)$$

The modeled equation of the TKE, k is written as:

$$\frac{\partial}{\partial x_i}(\rho k u_i) = \frac{\partial}{\partial x_j}\left[\left(\mu + \frac{\mu_t}{\sigma_k}\right)\frac{\partial k}{\partial x_j}\right] + G_k - \rho\varepsilon \qquad (7)$$

Similarly the dissipation rate of TKE, ε is given by the following equation:

$$\frac{\partial}{\partial x_i}(\rho \varepsilon u_i) = \frac{\partial}{\partial x_j}\left[\left(\mu + \frac{\mu_t}{\sigma_\varepsilon}\right)\frac{\partial \varepsilon}{\partial x_j}\right] + C_{1\varepsilon}\frac{\varepsilon}{k}G_k - C_{2\varepsilon}\rho\frac{\varepsilon^2}{k} \qquad (8)$$

where G_k is the rate of generation of the TKE while $\rho\varepsilon$ is its destruction rate.
G_k is written as:

$$G_K = -\rho u_i' u_j' \frac{\partial u_j}{\partial u_i} \qquad (9)$$

The boundary values for the turbulent quantities near the wall are specified with the enhanced wall treatment method. C_μ=0.09, $C_{1\varepsilon}$=1.44, $C_{2\varepsilon}$=1.92, σ_k=1.0, σ_ε=1.3 and Pr_t=0.9 are chosen to be empirical constants in the turbulence transport equations.

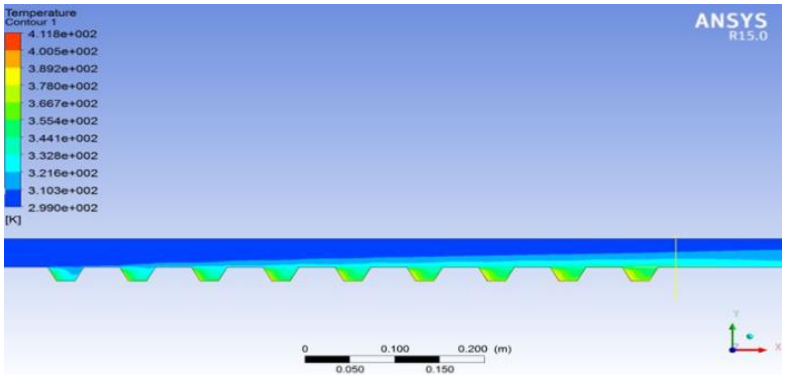

Fig.4 Contours of static temperature of fluid for grooved at Re = 6000 for B/H = 1

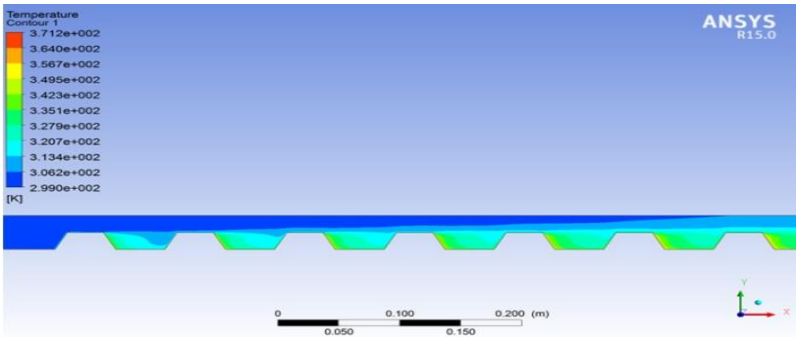

Fig.5 Contours of static temperature of fluid for ribbed at Re = 6000 for B/H = 1.25

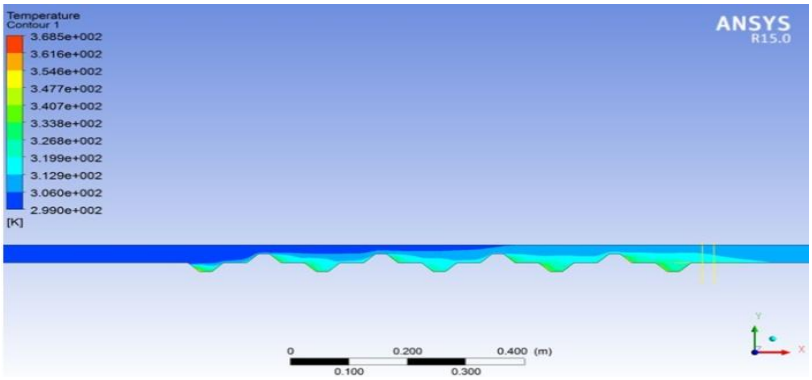

Fig.6 Contours of static temperature of fluid for rib-grooved at Re = 6000 for B/H = 1.5

3.2. Turbulence models

In contrast to the molecular viscosity, the eddy viscosity depends strongly on the flow property. Therefore, selecting the turbulence model, to accommodate the flow behavior of each application, is very important. To attain the accurate aerodynamic prediction in the grooved channel, the predictive ability of four different turbulence models, including the standard k−ε turbulence model the Renormalized Group (RNG) k−ε turbulence model, the standard k−ω turbulence model and
The Shear Stress Transport (SST) k−ω turbulence models are investigated.

3.3. Solution procedure

The time-independent incompressible Navier–Stokes equations and the turbulence model were discretized using the finite volume method QUICK (Quadratic upstream interpolation for convective kinetics differencing scheme) and central differencing flow numerical schemes were applied for convective and diffusive terms, respectively. The discretized nonlinear equations were implemented implicitly. To evaluate the pressure field, the pressure–velocity coupling algorithm SIMPLE (Semi Implicit Method for Pressure-Linked Equations) was selected. At the inlet, uniform velocity profile has been imposed. Impermeable boundary condition has been implemented over the channel wall while constant heat flux condition is applied to the lower wall of test section. The turbulence intensity was kept at 10% at the inlet.

Two parameters of interest for the present case are: (1) friction factor, (2) Nusselt number. The friction factor, f is computed by pressure drop, Δp across the length of test section, L, having the hydraulic diameter, D_h.

$$f = \frac{(\Delta p/L)D_h}{\frac{1}{2}\rho u^2} \qquad (10)$$

The heat transfer is measured by local Nusselt number which can be obtained by

$$Nu(x) = \frac{h(x)D_h}{k} \qquad (11)$$

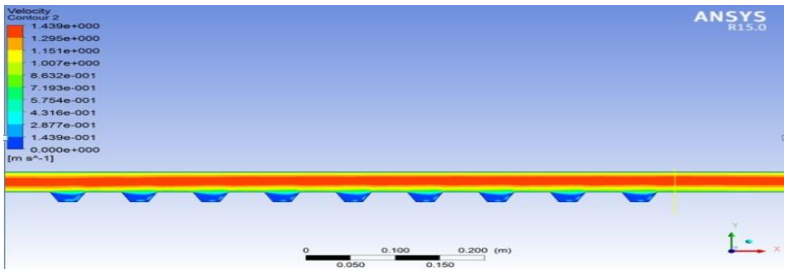

Fig.7 X-velocity contours at Re = 6000 for B/H = 1

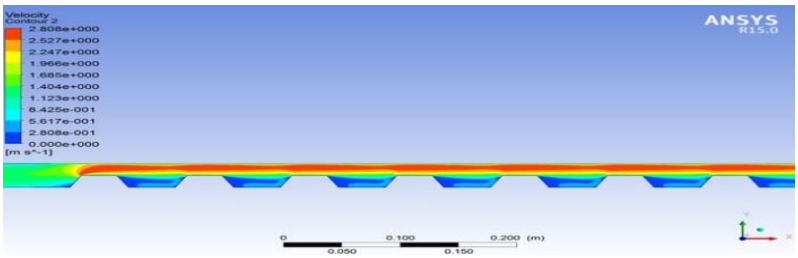

Fig.8 X-velocity contours at Re = 6000 for B/H = 1.25

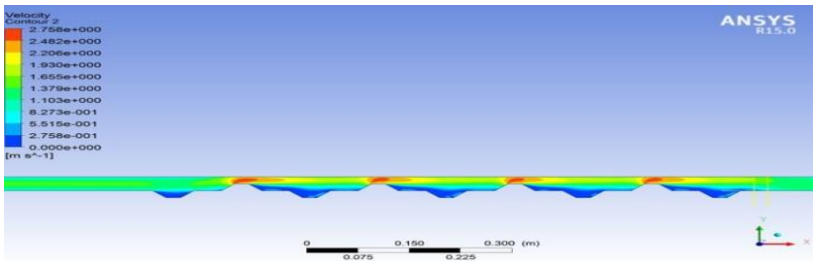

Fig.9 X-velocity contours at Re = 6000 for B/H = 1.5

III. NUMERICAL RESULTS

4.1. Effect of turbulence models

When compares the axial variation of surface Nusselt number along a single groove of one pitch of previous measured data [5] with the present work using various turbulence models (the standard k−ε model, the RNG k−ε model, the standard k−ω model and the SST k−ω model) at Re=12,000 and B/H=1.0. The average top surface Nusselt number of the channel with a groove is also shown in the figure. The numerical predicted result with the RNG k−ε turbulence model or the standard k−ε turbulence model agrees well with the experimental data [5] than that with the standard k−ω model or the SST k−ω model, except at l/H=1.5 to 2.0. The predicted and

measured results are in a similar trend for using both the RNG k−ε model and the standard k−ε model. Thus, any of the RNG k−ε model or the standard k−ε model appears to be suitable in prediction of this flow. The highest heat transfer rate is found on the top surface of rib or at l/H=0.5 to 1.5.

4.3. Flow structure

Fig.7-9 shows X-velocity contours at Re = 6000 for B/H ratio 1, 1.25 and 1.5 of trapezoidal grooved, ribbed and rib-grooved respectively. It can be visible that the largest re-circulation zone can be found in the groove region for B/H=1.5 the larger the groove, the longer becomes the re-circulation zone. The contour plots of turbulence kinetic energy are displayed in Fig. 7-9 for different width ratios (B/H). The peak turbulence intensity values, predicted by the k−ε turbulence model, are seen on the top of rib front regions, while the turbulence intensity is observed to be very low at groove bottom wall area. A large turbulence kinetic energy zone is found between the adjacent ribs close to the main flow which yields the strong influence of turbulence intensity on heat transfer enhancement.

4.4. Heat transfer

The comparison between Reynolds number and Nusselt number is presented in fig.10. From fig. it is observed that the maximum heat transfer occurred when the B/H ratio is 0.5. Fig.11 presents the heat transfer results for air flow in the channel for five different groove-width ratios (B/H=0.5, 0.75, 1.0, 1.25, and1.5). In the fig. 11 the mean Nusselt numbers are related as a function of Reynolds number. The result obtained from smooth channel is also plotted for comparison. The variation of average Nusselt number is also presented in the fig. 11 which shows that the Nusselt number.

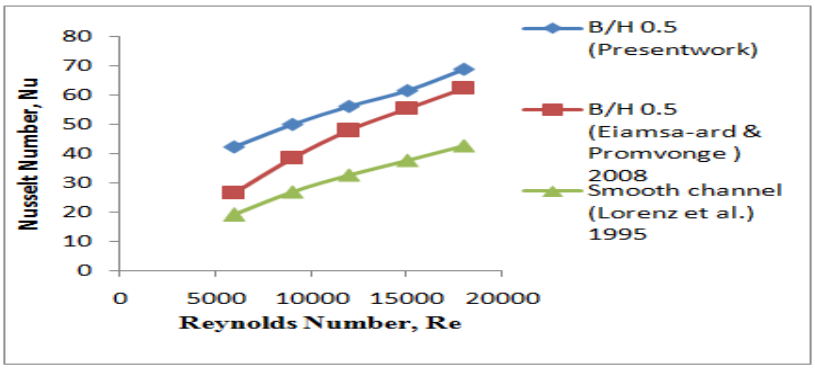

Fig.10 Validation of trapezoid grooved channel

Increases with the increase of Reynolds number. In all cases, the grooved channel flows give higher values of Nusselt number than that for smooth channel flow due to the induction of high re-circulation/reverse flow and thin boundary layer in the grooved channel, leading to higher temperature gradients.

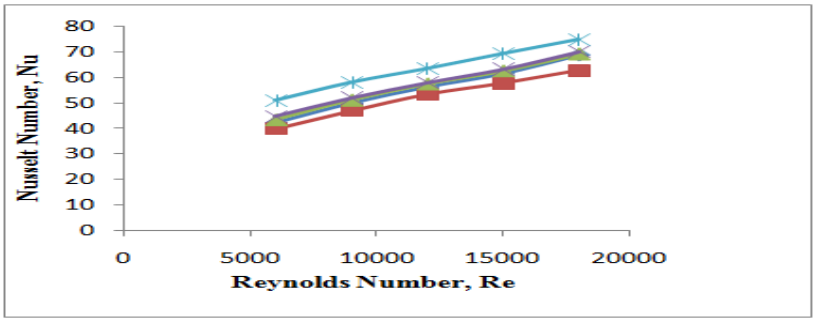

Fig.11 Variation of (Nu) with (Re) for trapezoid grooved channel

4.5. Friction loss

Fig. 12-14 shows the predicted results of friction factor using the k−ε turbulence model for different width ratios (B/H) in the range of Reynolds number investigated for fixed values of other parameters. It is seen that the friction factor decreases with increasing Reynolds number in all cases due to the suppression of viscous sub-layer with the increase of Reynolds number. The grooved channel is seen to yield higher friction factor than the smooth channel.

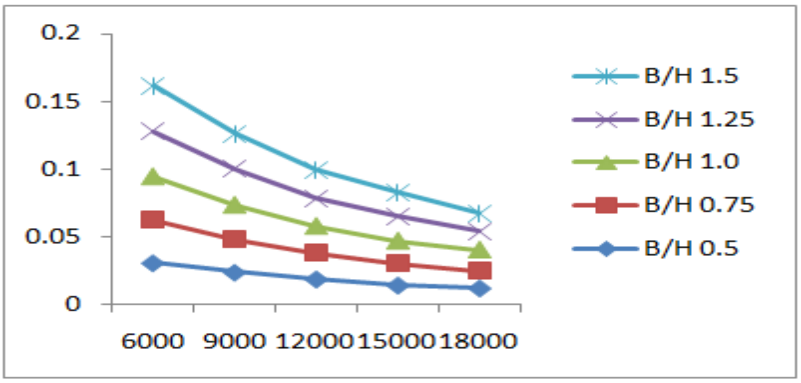

Fig. 12 Variation of friction factor with Reynolds number for grooved geometry

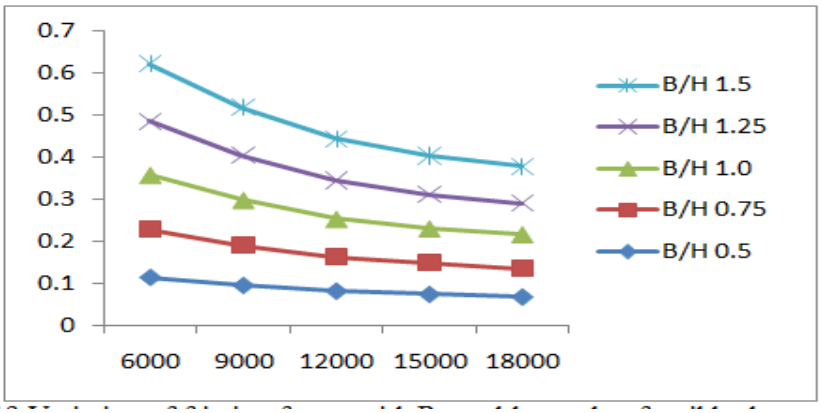

Fig.13 Variation of friction factor with Reynolds number for ribbed geometry

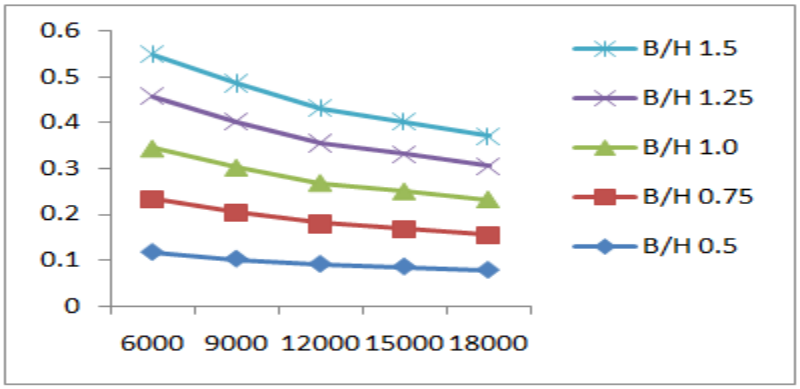

Fig.14 Variation of friction factor with Reynolds number for rib-grooved geometry.

The increase in Nusselt number values for using B/H=0.5, 0.75, 1.0, 1.25, and1.5, when compared with rectangular grooved channel shown in table 2.

Table 2: Showing increment in Nusselt number compared with rectangular grooved channel

Reynolds Number	B/H	Increment in Nusselt number %		
		Grooved	Ribbed	Rib-grooved
6000	0.5	20	3	Null
	0.75	11	Null	Null
	1.0	21	10	17
	1.25	26	8	20
	1.5	45	20	26

Table 3: Shows increment in Nusselt number compared with smooth channel

Reynolds	B/H	Increment in Nusselt number %

Number		Grooved	Ribbed	Rib-grooved
6000	0.5	96	207	178
	0.75	93	216	183
	1.0	102	226	211
	1.25	104	218	210
	1.5	116	241	212

Above table 3 shows Increment in Nusselt number for different trapezoid geometry when compared to smooth turbulent channel.

IV. CONCLUSIONS

In this present investigation, a numerical prediction has been conducted to study heat transfer and flow friction behaviors in turbulent channel flows over periodic trapezoidal grooves, ribbed and rib-grooved shape of bottom plate. Verification of the heat transfer of the groove channel is performed by comparing with the previous research under similar conditions. So finally result showed a trend of increase in heat transfer with the provision of different geometries of plate surface for same thermal boundary conditions. The increase of heat transfer however was not found to be proportional to increase in ratio B/H of the trapezoidal rib, groove and rib-groove respectively.

REFERENCES

[1]. M. Dalle Donne, L. Meyer, Turbulent convective heat transfer from rough surfaces with two-dimensional rectangular ribs, International Journal Heat and Mass Transfer 20 (1977) 583–620.
[2]. S.R. Martin, C.J. Bates, Small-probe-volume Laser Doppler Anemometry measurements of turbulent flow near the wall of a rib-roughened channel, Flow Measurement Instrumentation 3 (1992) 81–88.
[3]. Y.M. Hong, S.S. Hsieh, Heat transfer and friction factor measurement in ducts with staggered and inline ribs, Transaction ASME Journal Heat Transfer 115 (1993) 58–65.
[4]. A.R. Jaurker, J.S. Saini, B.K. Gandhi, Heat transfer and friction characteristics of rectangular solar air heater duct using rib–grooved artificial roughness, Solar Energy 80 (2006) 895–907.
[5]. S. Lorenz, D. Mukomilow, W. Leiner, Distribution of the heat transfer coefficient in a channel with periodic transverse grooves, Experimental Thermal and Fluid Science 11 (1995) 234–242.
[6]. A. Chaube, P.K. Sahoo, S.C. Solanki, Analysis of heat transfer augmentation and flow
[7]. characteristics due to rib roughness over absorber plate of a solar air heater, Renewable Energy 31 (2006) 317–331.
[8]. A. Saidi, B. Sunden, Numerical simulation of turbulent convective heat transfer in square ribbed ducts, Numerical Heat Transfer, Part A: Applications 38 (1) (2000) 67–88.
[9]. K. Tatsumi, H. Iwai, K. Inaoka, K. Suzuki, Numerical analysis for heat transfer characteristics of an oblique discrete rib mounted in a square duct, Numerical Heat Transfer, Part A: Applications 44 (8) (2003) 811–831.
[10]. Y.T. Yang, C.W. Hwang, Numerical calculations of heat transfer and friction characteristics in rectangular ducts with slit and solid ribs mounted on one wall, Numerical Heat Transfer, Part A: Applications 45 (4) (2004) 363–375.

*Rohit Joshi. "CFD Analysis for Thermal Behavior of Turbulent Channel Flow of Different Geometry of Bottom Plate." International Journal of Engineering Research and Development, vol. 13, no. 09, 2017, pp. 12–19.